

Formation of Field-Reversed-Configuration Plasma with Punctuated-Betatron-Orbit Electrons

D. R. Welch,¹ S. A. Cohen,² T. C. Genoni,¹ and A. H. Glasser³

¹*Voss Scientific, Albuquerque, New Mexico 87108, USA*

²*Princeton Plasma Physics Laboratory, Princeton, New Jersey 08544, USA*

³*Department of Aeronautics and Astronautics, University of Washington, Seattle, Washington 98195, USA*

(Received 6 January 2010; published 1 July 2010)

We describe *ab initio*, self-consistent, 3D, fully electromagnetic numerical simulations of current drive and field-reversed-configuration plasma formation by odd-parity rotating magnetic fields (RMF_o). Magnetic-separatrix formation and field reversal are attained from an initial mirror configuration. A population of punctuated-betatron-orbit electrons, generated by the RMF_o, carries the majority of the field-normal azimuthal electrical current responsible for field reversal. Appreciable current and plasma pressure exist outside the magnetic separatrix whose shape is modulated by the RMF_o phase. The predicted plasma density and electron energy distribution compare favorably with RMF_o experiments.

DOI: 10.1103/PhysRevLett.105.015002

PACS numbers: 52.55.Lf, 52.50.Qt, 52.55.Wq, 52.65.Rr

Electrical currents may be generated in magnetized plasma by a number of electrodeless methods. Inductive, radio-frequency-wave [1], energetic-beam-injection [2,3], and bootstrap [4] techniques are widely used to drive currents parallel to the magnetic field, while perpendicular currents may be generated by beam injection [5,6], diamagnetism, the thermoelectric effect [7], and rotating magnetic fields (RMFs) [8]. The latter group is particularly relevant to field-reversed-configuration (FRC) [9] plasma [see Fig. 1(a)], unique among toroidal plasma in having only a poloidal magnetic field and a magnetic null on the magnetic axis where the plasma energy density is highest. Producing current at the null is particularly difficult [7]. This paper provides physical insights and self-consistent calculations into a novel nonresonant radio-frequency technique whose symmetry properties promote direct generation of field-normal currents in FRCs, even on-axis.

FRC-like plasmas are frequent in planetary and astrophysical settings [10]. They are also created in the laboratory to study magnetic relaxation, reconnection [11], stability, and transport [12,13] and to explore FRCs as potential fusion reactors [14–16]. Many powerful methods of plasma theory, including magnetohydrodynamics, gyrofluid, drift-wave-instability [17], and even Taylor relaxation [18] models are deficient for FRC plasma because of the distinctive FRC properties [19]. Detailed understanding of and predictive capabilities for FRC plasma behavior require new theoretical tools.

RMFs, primarily of even parity (RMF_e), have been used to form and sustain FRC plasmas and to heat their electrons. Odd-parity RMFs (RMF_o) are predicted to perform the aforementioned and additional functions, such as heating ions [20], improving confinement [21], and increasing stability [22]. Recent experimental studies of RMF_o [15,23] have provided limited support for certain of these predictions. The new theoretical tools for FRCs must also properly treat RMF_o, which, among other effects, removes axial symmetry and adds a new characteristic time scale,

the rotational period, placing even more stringent demands on a plasma model. Herein, we describe specific reasons for a particle-in-cell (PIC) [24] method for modeling the RMF_o/FRC and results uncovered by using it. One important result is that the electrical current is not predominantly carried by smoothly drifting or circulating particles but by electrons whose trajectories alternate between fast-circulating, higher energy (low collisionality, ν) betatron orbits and slowly drifting, lower energy cyclotron orbits [25], with a net time-averaged azimuthal speed $\langle v_{\phi,e} \rangle$ nearly equal to the RMF_o's. This ratchetlike motion [see Fig. 1(b) and inset], which we term *punctuated* betatron orbits, has been observed in earlier single-particle simulations [20] but never before in a self-consistent simulation. Moreover, RMF_o current drive does not depend on a wave-particle resonance central to the high efficiency method of Fisch [26]; hence, it can operate at a slow wave phase velocity and still generate high-energy low- ν electrons.

A distinguishing feature of RMF_o is a time-varying azimuthal electric field ε_{ϕ} , generated near and on the plasma midplane ($z = 0$), which also contains the defining O -point field null line, the FRC's magnetic axis. Importantly, ε_{ϕ} has both clockwise and counterclockwise regions that rotate at ω_R , the RMF_o frequency [see Fig. 1(b)]. Cyclotron-orbit electrons in the clockwise region $E \times B$ drift towards the null line, become betatron orbits, and then accelerate along the null. These betatron-orbit electrons then enter the counterclockwise region, decelerate, become cyclotron orbits, and slowly drift away from the null line, waiting for the RMF_o to bring the clockwise ε_{ϕ} region back to them to begin the ratchetlike azimuthal motion anew.

Magnetohydrodynamics or gyrokinetic models cannot properly treat a null, the ε_{ϕ} -driven particle acceleration near the null line, or when either the ion or electron gyroradius $\rho_{i,e}$ is comparable to the separatrix radius r_s . Test-particle techniques can accurately model ion or electron dynamics but neglect the plasma response, such as whether the RMF_o penetrates the plasma, if RMF_o causes

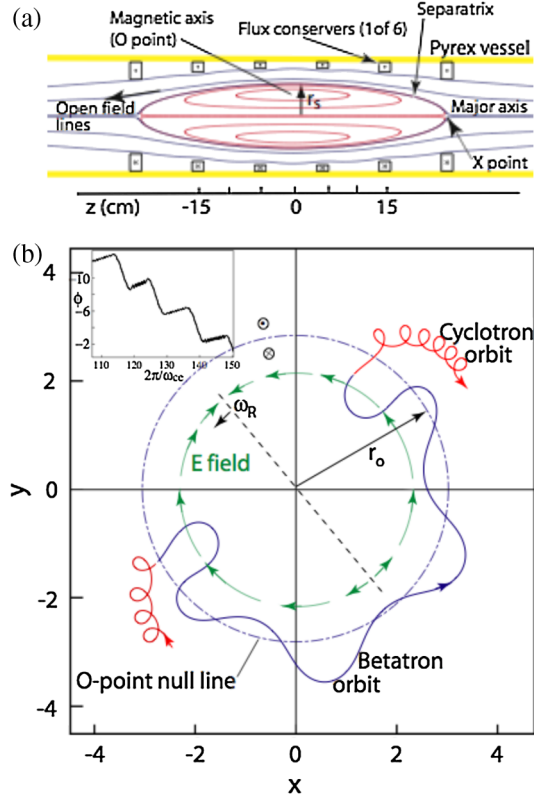


FIG. 1 (color online). (a) Midplane of the PFRC device with magnetic-field lines shown. Closed field lines are red. (b) An electron trajectory (blue when betatron and red when cyclotron). The O-point null line is an approximation. (Inset) Electron azimuthal position versus time.

the magnetic-flux-surface shape to evolve, or whether turbulence develops and alters plasma dynamics. PIC techniques avoid these deficiencies and provide the first fully self-consistent description of FRC formation from an initial low- β (ratio of plasma kinetic pressure to magnetic-field energy density) mirror plasma configuration.

For concreteness, we model a specific RMF_o device, the Princeton field-reversed configuration (PFRC) [15], sketched in Fig. 1(a). An 80-cm-long Pyrex cylinder is the vacuum vessel. Internal are 6 coaxial magnetic-flux-conserving copper rings (FC), three on each side of the midplane. External to the Pyrex vessel and symmetric about its midplane is the RMF_o antenna. Typical RMF_o characteristics are field strength $B_R \sim 10$ G and frequency $\omega_R/2\pi = 14$ MHz. At an axial field at the FRC's center of $B_a = 100$ G, $90\omega_{ci} \sim \omega_R \sim \omega_{ce}/20$, where $\omega_c = qB_a/mc$ is the particle cyclotron frequency, m is the particle mass, q is the particle charge, and subscripts e and i refer to electron and ion, respectively.

A static mirror-configuration magnetic field is created by coaxial coils located near $z = \pm 45$ cm and $z = \pm 105$ cm. Nominally, these coils produce an initial axial bias field of strength $B_o = 50$ G at $z = 0$ cm and 2000 kG at $z = \pm 45$ cm. A necessary goal is for the RMF_o to produce sufficient azimuthal plasma current to reverse

the magnetic field at $r = z = 0$ cm. When this occurs, the field ($B_a = -B_e$) at the FRC's center is about twice larger in magnitude than B_o . At the application of RMF_o power to the PFRC, the density rapidly rises. Within the first few microseconds, a near steady state is reached in which the plasma parameters are typically $n_e = 0.7 - 3 \times 10^{12}$ cm⁻³, $T_e = 300 - 100$ eV, and $T_i \sim 1$ eV.

PIC simulations, now described, were performed with the Large Scale Plasma (LSP) code [27,28]. LSP uses an explicit PIC algorithm, with standard particle-advance techniques augmented by a novel energy-conserving push [29] that avoids the so-called Debye-length numerical instability. LSP uses a temporally implicit, noniterative, unconditionally stable electromagnetic field solver [30] and a cloud-in-cell linear interpolation technique between particle locations and grid boundaries. Approximately 200 particles *per cell* are used for each particle species.

The RMF_o antennae are modeled with a sinusoidal current. The applied magnetic fields from the small- and large-bore coils at both ends of the PFRC are precalculated from a magnetostatic solution. Particles striking axial, radial, and FC boundaries are removed from the simulation.

The spatial extent of the LSP simulation is $r = \{0, 5\}$ cm, $\phi = \{0, 2\pi\}$, and $z = \{-50, +50\}$ cm, with grid spacings of $\Delta r = 0.15$ cm, $\Delta\phi = \pi/4$, and $\Delta z = 0.2$ cm. The explicit time-step limitation requires $\Delta t < \omega_{pe}^{-1} (\sim 10^{-11}$ s), corresponding to about 10^6 time steps. A typical simulation takes 4 days on a 32-processor cluster.

A simulation begins with an $n_e \sim 10^{11}$ cm⁻³, $T_e = 4$ eV hydrogen plasma seeded in the Pyrex vessel, along with room-temperature molecular hydrogen of density 3.5×10^{13} cm⁻³, corresponding to the PFRC fill pressure. The RMF_o causes acceleration of plasma electrons and ionization of the H₂ and, hence, plasma densification and electron heating. H₂⁺ is the dominant ion species formed in these relatively short simulations. Charged-particle collisions are treated by using Spitzer rates. Charged-neutral collisions are handled with a Monte Carlo method utilizing energy-dependent tabular cross sections σ . Scattering and ionization σ 's for $\bar{e} - H_2$ from the literature are employed; $\sigma_{H_2^+ - H_2^-}$ is assigned a constant 10^{-15} cm². Neutral-neutral collisions assumed an isotropic scattering cross section of 7×10^{-16} cm². LSP calculates energy losses by collective radiation, charge exchange, and ionization, as well as conduction and convection to boundaries. Simulations are typically for 5 μ s, during which time the neutral density drops about 1%.

Figure 2(a) shows the early time evolution of the total ion charge in the simulation volume for 5 values of the initial external field, $B_o = B_{z0} \equiv B_z(r, z, t)$ at $t = r = z = 0$, and $B_R = 10$ G. Positive B_{z0} values correspond to the correct B_o direction to form an FRC by the rotation sense of the RMF_o. The figure shows density increasing exponentially with time with higher plasma densities attained at higher B_{z0} , doubling as B_{z0} is increased from 35 to 100 G, consistent with experiment [15]. For positive B_{z0} , there is a

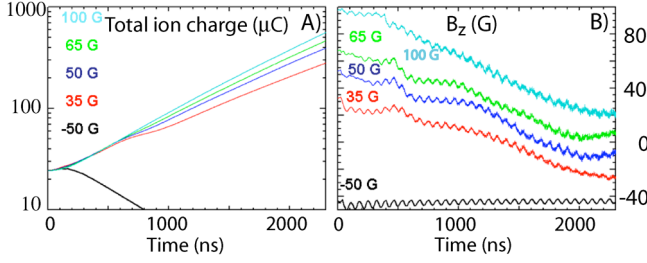


FIG. 2 (color online). (a) Total ion charge in the simulation volume versus time, for 5 values of the initial axial field B_{z0} . (b) Axial field strength at $z = 0$ and $r = 1$ cm versus time, for the same initial values of B_{z0} .

temporary decrease in the rate of density rise between 600 and 900 ns, an effect we attribute to increased radial particle losses. Density saturation occurs at about $5 \mu\text{s}$, with the exact time depending on fill pressure, B_R , etc. (For the $B_{z0} = 50$ G, $B_R = 10$ G case shown, the density at $5 \mu\text{s}$ is within 10% of that measured in the experiment.) When B_{z0} is negative, the density rises slightly for 50 ns and then decays similar to measurements on the PFRC. This critical simulation shows the importance of consistency between the sense of rotation and the initial B_o direction.

Figure 2(b) shows the axial field strength versus time at $z = 0$ and $r = 1$ cm for the five values of B_{z0} . For positive B_{z0} , the axial field strength falls with time and reverses for the lower B_{z0} values. The oscillations in B_z are at the RMF_o frequency and are due to the proximity of the RMF_o antenna's central arm. A fuller appreciation of field reversal can be gained from Fig. 3, which presents snapshots in the r - z plane of three parameters, n_e , T_e , and B_z , at 5 times during the simulation with $B_{z0} = 50$ G. The top row shows n_e . Though the total number of ions grows over the entire $2.5 \mu\text{s}$ period displayed, the radial location of the sharp density gradient shrinks between 50 and 375 ns and then grows until 1000 ns, by which time it reaches 3 cm. After $t = 1 \mu\text{s}$, the n_e profile expands axially at a speed of 2.3×10^7 cm/s, about twice the ion acoustic speed.

The middle row shows T_e (defined as $2/3$ of the average electron energy) rapidly rising, reaching over 250 eV in isolated regions beginning at $t \sim 400$ ns. For the next 500 ns, 50% variations in T_e occur over 1-cm-scale—com-

parable to $\rho_{e,i}$ and c/ω_{pe} —axial and radial distances at a frequency above 200 MHz. (ω_{pe} is the electron plasma frequency.) This turbulent period is concurrent with the aforementioned decrease in the density rate of rise and is coincident with a large value for the drift parameter, $\gamma_D = \langle v_{\phi,e} \rangle / \text{ion thermal speed} \sim 50$. As n_e continues to rise, T_e becomes more homogenous, settling at about 125 eV at $1 \mu\text{s}$. Electron energy fluctuations still occur at a reduced level, ca. $\pm 5\%$. The T_e profile inside the FC radius is nearly flat.

The bottom row shows the axial field. In the first $0.5 \mu\text{s}$, little change occurs in B_z , but by $t = 1 \mu\text{s}$, a 50% decrease is seen for $r < 2$ cm and $|z| < 10$ cm. At $t = 1.5 \mu\text{s}$, the azimuthal current has driven the central-region B_z to near zero. At $t = 2.5 \mu\text{s}$, field reversal is clearly evident in the region $r < 1$ cm, $|z| < 8$ cm.

Local projections of the magnetic field, i.e., contours of $\hat{r}B_r + \hat{z}B_z$ (iron-filing plots), onto two orthogonal r - z planes at $t = 2 \mu\text{s}$ are presented in Fig. 4(a). In both planes, a fully developed FRC is inferred, with O -point nulls at $r_o = 1.6$ and 2 cm and $r_s = 3.1$ cm, to be compared with $r_s = 1.9$ – 3.0 cm reported in Ref. [15]. The FRC shape strongly changes with RMF_o phase, as predicted by Ref. [21]. In conjunction with Fig. 3, these data show a wide scrape-off layer and appreciable plasma pressure outside the separatrix. The changing shape of the separatrix and the oscillating position of the null repeat the intriguing question of whether this dynamic variation in the plasma's shape may improve the configuration's stability against the internal tilt mode [22]. Exploration of this question will require far longer simulations and a different set of plasma parameters, e.g., higher $r_s \omega_{pi} / Ec$, lower ν , and lower B_R / B_a .

Figure 4(b) shows an iron-filing plot of $\hat{r}B_r + \hat{\phi}B_\phi$ in the r - ϕ plane at $z = 7$ cm, $t = 2 \mu\text{s}$. These local projections imply RMF_o “penetration” to the FRC major axis. The field projections are twisted nearly 90° at $r \sim 2$ cm, possibly by electron drag on the ions or, as we estimate, more likely on the neutrals. For RMF_e and the assumption of Spitzer resistivity, full penetration [31] is predicted to occur when $P \equiv \gamma_c / \lambda > 2$, where λ is the ratio of r_s to the classical skin depth δ , and γ_c is the ratio of ω_R to ν . Including only electron-ion collisions $P \sim 6$. P falls to 1 adding electron-neutral collisions.

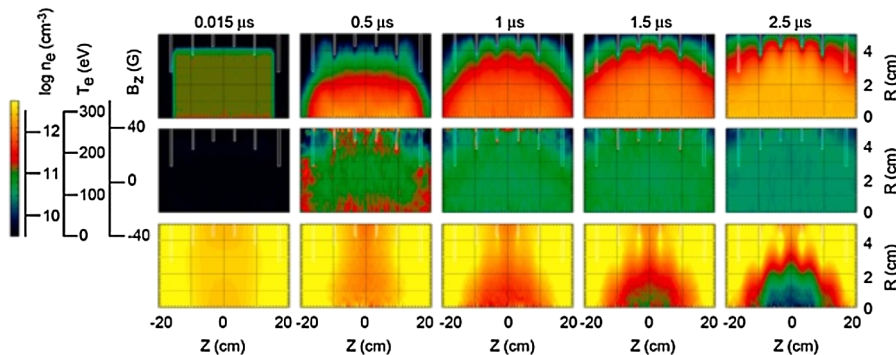


FIG. 3 (color online). Top row: $\log_{10} n_e$ (cm⁻³). Middle row: T_e (eV). Bottom row: B_z (G). The five columns are snapshots at the following times, from left to right: 0.015, 0.5, 1, 1.5, and $2.5 \mu\text{s}$. Color-contour scales are to the left. The plasma shape is modulated by the flux conservers.

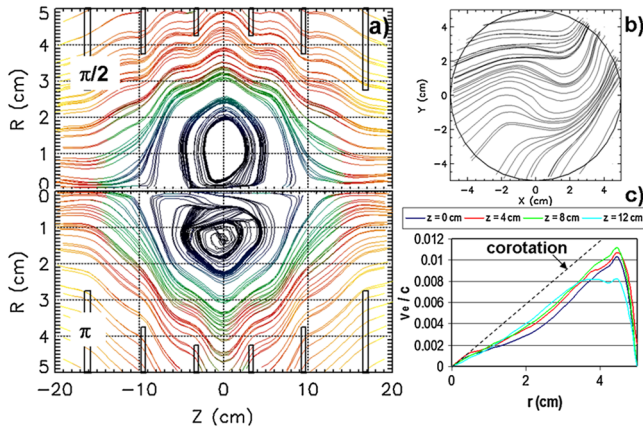


FIG. 4 (color online). At $t = 2 \mu\text{s}$ (a) local projections of magnetic-field lines in the r - z plane for two RMF phases, 90° apart, and (b) local projections of field lines at $z = 7$ cm in the r - ϕ plane. (c) Average electron azimuthal velocity at four z locations (± 2 cm). The dashed line shows $\omega_R r/c$.

Figure 4(c) shows $\langle v_{\phi,e} \rangle / c$ versus radius for four axial positions, $z = 0, 4, 8, 12$ cm, ± 2 cm, at $t = 2 \mu\text{s}$: $\langle v_{\phi,e} \rangle$ ranges from 50% to 100% of the RMF₀ speed $\omega_R r$, with electrons on-axis and at larger radii having the higher percentage. Appreciable plasma current exists outside the separatrix because of the high $\langle v_{\phi,e} \rangle$ and n_e there. Inspection of hundreds of individual randomly selected superparticle trajectories from these PIC simulations show that punctuated betatron-orbit electrons contribute about 70% of the current for these low- s RMF₀/FRCs.

The calculated electron energy distribution function (EEDF) at $t = 2 \mu\text{s}$ is well characterized by a single 120-eV exponential from 100 eV to 1 keV. Above 1 keV a higher energy tail, ca. 180 eV, appears that is a far better fit to the experimental data than the Hamiltonian results [15], which showed a sharp cutoff in the EEDF at ~ 700 eV. This non-Maxwellian feature cannot be modeled by a fluid.

In summary, a 3D PIC plasma simulation technique has been applied to the study of FRC formation and electron heating by RMF₀. While the net current flows smoothly, individual electrons responsible for the majority of the plasma current have a ratchetlike azimuthal motion, characterized by punctuated-betatron-orbit trajectories. This method of current drive has the potential for high efficiency because of the high energy (low ν) of the current-carrying particles. Periods of large amplitude, high frequency, and short wavelength fluctuations in electron energy were observed and correlated with reduced density increase rate. The PIC results agreed well with the measured plasma density, electron temperature, EEDF, and separatrix location and also showed appreciable plasma pressure and azimuthal current outside the separatrix, whose shape was strongly modulated by both the flux conservers and the RMF₀ phase. These observations have strong ramifications for plasma transport and stability.

This work was supported, in part, by U.S. Department of Energy Contract No. DE-AC02-76-CHO-3073. We acknowledge helpful discussions with Donald Voss and code assistance from Robert Clark, Christopher Mostrom, and Clayton Myers.

- [1] N. Fisch, *Rev. Mod. Phys.* **59**, 175 (1987).
- [2] T. Ohkawa, *Nucl. Fusion* **10**, 185 (1970).
- [3] T. H. Stix, *Plasma Phys.* **14**, 367 (1972).
- [4] R. J. Bickerton, J. W. Connor, and J. B. Taylor, *Nature (London)*, *Phys. Sci.* **229**, 110 (1971).
- [5] N. C. Christofilos, in *Proceedings of the 2nd International UN Conference on Peaceful Uses of Atomic Energy (Geneva)* (United Nations, New York, 1958), Vol. 32, p. 279.
- [6] H. H. Fleischmann, *Ann. N.Y. Acad. Sci.* **251**, 472 (1975).
- [7] A. B. Hassam, R. M. Kulsrud, R. J. Goldston, H. Ji, and M. Yamada, *Phys. Rev. Lett.* **83**, 2969 (1999).
- [8] H. A. Blevin and P. C. Thonemann, *Nucl. Fusion Suppl.* Pt. **1**, 55 (1962).
- [9] M. Tuszewski, *Nucl. Fusion* **28**, 2033 (1988).
- [10] P. M. Bellan, *Spheromaks* (Imperial College Press, London, 2000).
- [11] E. Kawamori and Y. Ono, *Phys. Rev. Lett.* **95**, 085003 (2005).
- [12] H. Y. Guo, A. L. Hoffman, L. Steinhauer, and K. E. Miller, *Phys. Rev. Lett.* **95**, 175001 (2005).
- [13] L. C. Steinhauer and T. P. Intrator, *Phys. Plasmas* **16**, 072501 (2009).
- [14] J. Slough *et al.*, *J. Fusion Energy* **26**, 199 (2007).
- [15] S. A. Cohen *et al.*, *Phys. Rev. Lett.* **98**, 145002 (2007).
- [16] N. Rostoker, A. Qerushi, and M. Binderbauer, *J. Fusion Energy* **22**, 83 (2003).
- [17] N. C. Krall and P. C. Liewer, *Phys. Rev. A* **4**, 2094 (1971).
- [18] J. B. Taylor, *Phys. Rev. Lett.* **33**, 1139 (1974).
- [19] J. L. Schwarzmeier and C. E. Seyler, *Phys. Fluids* **27**, 2151 (1984).
- [20] A. H. Glasser and S. A. Cohen, *Phys. Plasmas* **9**, 2093 (2002).
- [21] S. A. Cohen and R. D. Milroy, *Phys. Plasmas* **7**, 2539 (2000).
- [22] S. A. Cohen, *Bull. Am. Phys. Soc.* **44**, 596 (1999).
- [23] H. Y. Guo *et al.*, *Phys. Rev. Lett.* **94**, 185001 (2005).
- [24] C. K. Birdsall and A. B. Langdon, *Plasma Physics via Computer Simulation* (McGraw-Hill, New York, 1985).
- [25] A. S. Landsman, S. A. Cohen, and A. H. Glasser, *Phys. Plasmas* **11**, 947 (2004).
- [26] N. Fisch, *Phys. Rev. Lett.* **41**, 873 (1978).
- [27] LSP is a software product of ATK Mission Research, Albuquerque, NM 87110.
- [28] T. P. Hughes, S. S. Yu, and R. E. Clark, *Phys. Rev. ST Accel. Beams* **2**, 110401 (1999).
- [29] D. R. Welch, D. Rose, M. Cuneo, R. Campbell, and T. Mehlhorn, *Phys. Plasmas* **13**, 063105 (2006).
- [30] D. R. Welch *et al.*, *Comput. Phys. Commun.* **164**, 183 (2004).
- [31] W. N. Hugrass and R. C. Grimm, *J. Plasma Phys.* **26**, 455 (1981).